AUTHOR(S): NAGARAJAN, S., SKILLEN, N.C., FINA, F., ZHANG, G., RANDORN, C., LAWTON, L.A., IRVINE, J.T.S. and ROBERTSON, P.K.J.

TITLE: Comparative assessment of visible light and UV active photocatalysts by hydroxyl radical quantification.

YEAR: 2016

Publisher citation: NAGARAJAN, S., SKILLEN, N.C., FINA, F., ZHANG, G., RANDORN, C., LAWTON, L.A., IRVINE, J.T.S. and ROBERTSON, P.K.J. 2016. Comparative assessment of visible light and UV active photocatalysts by hydroxyl radical quantification. Journal of photochemistry and photobiology A: chemistry [online], 334, pages 13-19. Available from: http://dx.doi.org/10.1016/j.jphotochem.2016.10.034

OpenAIR citation: NAGARAJAN, S., SKILLEN, N.C., FINA, F., ZHANG, G., RANDORN, C., LAWTON, L.A., IRVINE, J.T.S. and ROBERTSON, P.K.J. 2016. Comparative assessment of visible light and UV active photocatalysts by hydroxyl radical quantification. Journal of photochemistry and photobiology A: chemistry, 334, pages 13-19. Held on OpenAIR [online]. Available from: https://openair.rgu.ac.uk/

Comparative assessment of visible light and UV active photocatalysts by hydroxyl radical quantification

Sanjay Nagarajan[1]*, Nathan C. Skillen[1], Federica Fina[2], Guan Zhang[2], Chamnan Randorn[2], Linda A. Lawton[3], John T.S. Irvine[2] and Peter K.J. Robertson[1]*

[1] Centre for the Theory and Application of Catalysis (CenTACat), School of Chemistry and Chemical Engineering, Queen's University Belfast, David Keir Building, Stranmillis Road, Belfast, BT9 5AG, United Kingdom;

[2] JTSI Group, University of St. Andrews, School of Chemistry, Purdie Building, North Haugh, St Andrews, KY16 9ST, United Kingdom;

[3]School of Pharmacy and Life sciences, Sir Ian Wood Building Robert Gordon University, Garthdee Road, Aberdeen, AB10 7GJ, United Kingdom

*Corresponding authors, *p.robertson@qub.ac.uk;* snagarajan01@qub.ac.uk*, Tel: +44 (0) 28 9097 4627*

ABSTRACT

A simple method for determining hydroxyl radical yields on semiconductor photocatalysts is highly desirable, especially when comparing different photocatalyst materials. This paper reports the screening of a selection of visible light active photocatalysts such as Pt-C_3N_4, 5% LaCr doped $SrTiO_3$, $Sr_{0.95}Cr_{0.05}TiO_3$ and Yellow TiO_2 and compares them against WO_3 and ultra violet (UV) light activated TiO_2 P25 (standard commercial catalysts) based on their oxidative strengths (OH radical producing capability) using a well-studied chemical probe – coumarin. 7-hydroxycoumarin, the only fluorescent hydroxylation product of this reaction can then be measured to indirectly quantify the OH radicals produced. P25 under UV light produced the highest concentration of OH radicals (16.9 µM), followed by WO_3 (0.56 µM) and Pt-C_3N_4 (0.25 µM). The maximum OH radical production rate for P25, WO_3

and Pt-C_3N_4 were also determined and found to be 35.6 µM/hr, 0.28 µM/hr and 0.88 µM/hr respectively. The other visible light activated photocatalysts did not produce any OH radicals primarily as a result of their electronic structure. Furthermore, it was concluded that, if any visible light absorbing photocatalysts are to be fabricated in future for the purpose of photocatalytic oxidation, their OH radical producing rates (and quantities) should be determined and compared to P25.

Keywords: Photocatalyst, visible light photocatalysts, OH radical, coumarin, P25.

1. INTRODUCTION

Photocatalysis has gained significant interest since the early publication by Fujishima and Honda in 1972, demonstrating the potential of splitting water over TiO_2 [1]. Since this publication, photocatalysis has been applied to a broad range of fields including waste water treatment, microbe destruction, toxin removal, energy production and air treatment. [2-8]. The mechanism of photocatalysis has been well documented and can be generally represented by the equations shown in reactions 1-9 [9,10]. The formation of surface radical species such as superoxide ($O_2^{\cdot -}$) and hydroxyl radicals ($OH^{\cdot}$) play a key role in a number of photocatalytic pathways and as such their identification and quantification is a key consideration. As shown in reaction 2, OH radicals are primarily generated from the reaction between valence band holes (h_{vb+}) and hydroxyl ions on the catalyst surface. An indirect pathway, via $O_2^{\cdot -}$, also results in OH radical formation, as shown in reactions 3-6. The efficiency of OH radicals in photocatalytic reactions is predominantly based on their strong oxidising potential of 2.8 V (vs NHE) [11]. The non-selective nature of these reactive oxygen species also aids rapid degradation of various pollutants and organic contaminants [3,7,11-16].

$$Photocatalyst \quad + h\nu \ \rightarrow \quad h_{vb^+} + e_{cb^-} \qquad \ldots\ldots\ldots\ldots\ldots\ldots (1)$$

$$h_{vb^+} + OH^-(or\ H_2O) \rightarrow OH^{\cdot} \qquad \ldots\ldots\ldots\ldots\ldots\ldots (2)$$

$$e_{cb^-} + O_2 \rightarrow O_2^{-\cdot} \qquad \ldots\ldots\ldots\ldots\ldots\ldots (3)$$

$$O_2^{-\cdot} + H^+ \rightarrow HO_2^{\cdot} \qquad \ldots\ldots\ldots\ldots\ldots\ldots (4)$$

$$HO_2^{\cdot} + HO_2^{\cdot} \rightarrow H_2O_2 + O_2 \qquad \ldots\ldots\ldots\ldots\ldots\ldots (5)$$

$$H_2O_2 + e_{cb^-} \rightarrow OH^{\cdot} + OH^- \qquad \ldots\ldots\ldots\ldots\ldots\ldots (6)$$

$$O_2^{-\cdot} + reactants \rightarrow products \qquad \ldots\ldots\ldots\ldots\ldots\ldots (7)$$

$$substrates + \cdot OH \rightarrow products \qquad \ldots\ldots\ldots\ldots\ldots\ldots (8)$$

$$e_{cb^-} + OH^{\cdot} \rightarrow OH^- \quad \text{...} \ (9)$$

where, h_{vb}^+ represents VB holes and e_{cb}^- means CB electrons.

Newly developed photocatalytic technologies and materials have often utilised model compounds and screening methods to assess their performance [17-20]. Common evaluation methods reported in the literature include the decomposition of dyes such as methylene blue (ISO test 10678:2010), or degradation of organic pollutants such as 4-chlorophenol or toluene [17-20]. These procedures are often coupled with the corresponding calculated photonic efficiencies and quantum yields to evaluate overall efficiency. While these methods can be effective in identifying the specific photocatalytic performance of a material in relation to a fingerprint compound, they provide little information regarding the production of OH radicals involved within the mechanism. Therefore, the requirement for a simple and robust method of radical quantification for screening the oxidative potential of catalysts has significantly increased. The challenge in OH radical quantification lies in both the non-selective nature and short lifetime (~ 1 nanosecond) of the radical, which restricts the possibility of direct quantification [21]. Consequently, a range of methods have been developed such as emission spectroscopy, laser induced fluorescence, electron spin resonance, spin trap and chemical probes or quencher based methods to quantify OH radicals [21-37].

The use of a chemical probe to capture OH radicals presents a potentially efficient way to measure the radical due to the low cost, rapid analysis time and reproducibility of the method. Monitoring a probe compound through spectroscopy allows the concentration of OH radicals to be calculated based on stoichiometric ratios of products formed. A recently reported *in vivo* technique utilised a nanoprobe comprising of a nanoparticle and azo dye in order to quantify OH radicals in the femtomolar range [37].

Here the nanoparticle was used as an energy donor and the modified orange was used as an OH radical capturing ligand molecule (and the energy acceptor).

Dimethyl sulfoxide (DMSO) based methods for OH radical capture have also been utilised in the past to quantify these species via the formation of formaldehyde [28,29,31]. The formation of CH_4 in a closed system coupled with O_2 bubbling however reduces the suitability of utilising DMSO as a probe molecule.

In the past, OH radical quantification has been carried out for various commercially available photocatalysts, photo-Fenton's reaction and other modified TiO_2 based visible light photocatalysts with either coumarin or terepthalic acid as probe molecules [21,23,31-36,38,39]. Both compounds are capable of acting as OH radical traps by forming fluorescent products as result of reacting with the radical species. Terepthalic acid has been investigated in a study by Ishibashi *et al*. which achieved an OH radical concentration of 7×10^{-5} M based on the measurement of 2-hydroxyterepthalic acid [35]. In addition to the use of terepthalic acid as a probe molecule, coumarin has been used in a number of studies to determine the concentration of OH radicals produced from TiO_2 at relatively high loadings of 1 to 5 g/L [21,23,40]. For instance, Czili *et al*. used 100 µM coumarin as the probe molecule to capture OH radicals under a 40 W UV lamp. They determined a maximum OH radical production rate of 23.39 µM/g/hr (calculated from their reported 7-hydroxycoumarin rates) with 1 g/L TiO_2 P25 photocatalyst.

This paper utilises coumarin as a hydroxyl radical trap and reports the screening of a selection of visible light responsive photocatalysts under low power illumination based on their OH radical producing capability. In contrast to previous reports, which concentrated on quantifying the OH radicals produced from TiO_2, other commercially available and a few synthesised photocatalysts [21,23,31,40], this work focusses on assessing the oxidative strength of visible light photocatalytsts Pt-C_3N_4, 5% LaCr doped $SrTiO_3$, $Sr_{0.95}Cr_{0.05}TiO_3$ (referred to as Cr-$SrTiO_3$ from here on) and yellow TiO_2 and compares them against commercial TiO_2 P25 and WO_3 for evaluation. In addition, a low catalyst loading was used to highlight efficient OH radical formation can be achieved without requiring large quantities of powdered catalyst.

2. EXPERIMENTAL PROCEDURE

2.1 Materials

Coumarin and 7-hydroxycoumarin were purchased from Tokyo Chemical Industry UK Ltd, while TiO_2 P25 was purchased from Degussa (now Evonik industries) and WO_3 nano powders were purchased from Sigma Aldrich. All commercial chemicals were used as received. The catalysts Pt-C_3N_4 [41], 5% LaCr doped $SrTiO_3$, Cr-$SrTiO_3$ and yellow TiO_2 [42] were synthesised at the school of chemistry, University of St. Andrews, using methods cited in the literature [41-43].

2.2 Characterisation of Photocatalysts

WO_3, LaCr-$SrTiO_3$ and Cr-$SrTiO_3$ were characterised by X-Ray diffraction (XRD) and UV-Visible absorption. XRD analysis of powders was examined on a SToe STADI/P powder diffractometer. Incident radiation was generated using a Cu k_α source (λ=1.54056 Å). Diffuse reflectance spectra were collected on a JASCO-V550 UV-visible spectrophotometer. The characterisation of Pt-C_3N_4 and yellow TiO_2 has been reported elsewhere in literature [41,42].

2.3 Photocatalytic experiments

All photocatalytic experiments were performed in closed screw cap bottles. The reaction solution was composed of 100 ml of 100 μM coumarin along with 10 mg of photocatalyst (0.1 g/L). A magnetic stirrer bar was placed inside the bottle and the bottle was then placed on a magnetic stirrer at a distance of 11 cm from a 36 W compact fluorescent non-integrated visible lamp (Philips, colour code 830) or a 36 W UV lamp (Philips, Cleo lamps). The spectral outputs of the lamps were measured by a StellaNet spectrometer and the spectra are shown in the supplementary material (Figure S1). Prior to illumination, the reaction solution was stirred in the dark to allow a state of equilibrium to be reached. The length of time required in the dark was calculated from the control experiments conducted in the absence of light. During irradiation, samples (3 mL) were taken at dedicated time intervals for a maximum of 120 mins. Samples were filtered through a 0.22 μm Millex syringe filter prior to analysis. Coumarin absorbance was monitored using a Cary 300 Scan, UV-Visible Spectrophotometer at 277 nm, with a scan rate of 400 nm/min. 7-hydroxycoumarin fluorescence was measured in a PerkinElmer LS 50B luminescence spectrophotometer, using an excitation wavelength of 332 nm and emission wavelength at 456 nm [21]. The excitation and emission slit width was 4 mm and the scan rate was 200 nm/min. A sample UV/Visible and fluorimeter spectra, with peaks at 277 nm and 456 nm respectively, are shown in the supplementary material Figure S2 and Figure S3. All experiments were performed in triplicate.

2.4 OH radical quantification

OH radicals were quantified based on a modified method described by Zhang *et al.* [38] and according to equation 1. The concentration of OH radicals was calculated by assuming that 6.1 % of total OH radicals were captured as 7-hydroxycoumarin. The stoichiometric ratio of one mole of OH radical consumed for the production of one mole of 7-hydroxycoumarin was used [23]. The total number of OH radicals produced over time during this photocatalytic process was calculated using the following equation.

$$X = \{\frac{A}{6.1\%} - B\}$$ .... Equation 1

Where, X is the total OH radical concentration (μM) produced during photocatalysis, A is the mean 7-hydroxycoumarin concentration (μM) and B is the amount of OH radicals (μM) produced during the light control experiments. The concentration of coumarin and 7-hydroxycoumarin was calculated using a standard curve of known concentrations as shown in the supplementary material (Figure S4, Figure S5 and Figure S6).

3. RESULTS AND DISCUSSION

3.1 Characterisation of Photocatalysts

XRD patterns of WO_3, Cr-$SrTiO_3$ and LaCr-$SrTiO_3$ samples were determined as shown (Figure 1). The commercial WO_3 nanoparticles exhibited a typical crystallized monoclinic phase structure, and the Cr-doped and La,Cr-co-doped $SrTiO_3$ samples possessed homogeneous crystallized cubic perovskite structures, with no impurity phase found for either of the doped samples and these results were consistent with literature [44,45]. In the co-doped samples, since La and Cr substitute the Sr and Ti, respectively, and the radius of La is similar with that of Sr while the radius of Cr was similar to that of Ti, the peak positions of the Cr-$SrTiO_3$ and LaCr-$SrTiO_3$ samples are not shifted compared to those of pure $SrTiO_3$.

Figure 1.

In the UV−visible absorption spectra of WO_3, Cr-$SrTiO_3$ and LaCr-$SrTiO_3$ (Figure 2), WO_3 exhibited visible light absorption up to 470 nm, which corresponds to the band-gap energy of ca. 2.64 eV. $SrTiO_3$, however, has no absorption in the visible light region (bandgap of 3.75 eV) and metal-doping has been shown to be a feasible method for extending the light absorption of $SrTiO_3$ into the visible region [46]. Doping of Cr into the A-site of $SrTiO_3$ induces an absorption band in the visible region centred at around 450 nm (Figure 2). The visible light absorption is ascribed to the electron excitation from the Cr doping levels formed above the valence band of $SrTiO_3$ to the conduction band of $SrTiO_3$ [43]. It was reported that La, Cr- co-doped $SrTiO_3$ showed enhanced photocatalytic performance compared to the single Cr-doped $SrTiO_3$ due to the inhibition of the formation of Cr^{6+} species in the B site [43]. Therefore, a co-doped sample, LaCr-$SrTiO_3$ was prepared by the same method. The visible light absorption of LaCr-$SrTiO_3$ was significantly enhanced compared to the Cr-$SrTiO_3$, with two strong absorption peaks centred at around 450 nm and 650 nm in the visible light region. In the case of co-doping, more intermittent doping levels are formed within the band-gap of $SrTiO_3$ compared to the single Cr doped $SrTiO_3$, which results in the visible light absorption.

Figure 2.

3.2 Photocatalytic OH radical production

3.2.1 UV light photocatalysis on P25

P25 has been one of the most extensively investigated and most active commercially available photocatalysts under UV irradiation and therefore was used as a benchmark for comparison in this study. Although, recent studies have reported that nano-spherical $InCrO_4$-loaded TiO_2 and TiO_2 nanospheres deposited on graphene performed better than P25 for OH radical production and dye degradation upon UV irradiation [47,48], to date P25 is still regarded as the benchmark. The photocatalytic hydroxylation of coumarin over P25 under UV light and subsequent formation of 7-hydroxycoumarin is shown in Figure 3. The production of 7-hydroxycoumarin under these conditions equates to a peak OH radical concentration of 16.9 µM after 45 mins.

Figure 3.

As shown in the figure, near complete degradation (97 %) of coumarin was achieved after 120 mins irradiation. This level of degradation was likely to result from the increased adsorption of coumarin onto the catalyst, which facilitated the reaction with surface bound OH radicals. The role of surface bound radicals and those that are present in bulk has been highlighted in a previous publication by Li *et al.* [49], who investigated acid orange oxidation over TiO_2 P25 and AgBr. This group investigated the quenching of OH radicals at the catalyst surface and in bulk in order to demonstrate that surface bound species were the predominant radicals in the oxidation pathway. This observation confirmed that increased adsorption of the substrate on the catalyst surface can significantly increase the degradation efficiency.

Figure 3 also shows the profile of 7-hydroxycoumarin production and decomposition which indirectly indicates the quantity of OH radicals generated. 7-hydroxycoumarin concentration peaked at 45 minutes, with a maximum concentration of 1.045 µM, which was equivalent to 16.9 µM OH radicals (as calculated from equation 1). It was observed that an average production rate of 1.8 µM/hr was achieved during the first 45 mins, followed by an average degradation rate of 0.46 µM/hr during the latter stages of irradiation. The decrease in concentration of 7-hydroxycoumarin could also be attributed to the presence of superoxide radicals as reported by Czili and Horvath [23].

Several reports have suggested the kinetics for 7-hydroxycoumarin generation from coumarin with P25 under UV irradiation are zero order [21,23,38,50-52], however, a number of these investigations also used a high concentration of both catalyst and coumarin. Furthermore, it has been suggested that at higher concentrations of coumarin (>100 µM), more UV light is absorbed by this probe and not the catalyst, which results in a low 7-hydroxycoumarin and OH radical production rate [23]. In the present study, K_{app} which is the rate constant for the formation of 7-hydroxycoumarin was calculated to be 0.0234 µM/min whereas K_{dis}, the rate constant for the disappearance of 7-hydroxycoumarin was calculated to be 0.0135 µM/min. In this study we have established that both, production and degradation of 7-hydroxycoumarin followed zero order kinetics, which is agreement with previous studies.

3.2.2 Visible light photocatalysis

A number of visible light catalysts were also selected for comparison against P25 TiO_2. While the synthesised catalysts all possessed energy band gaps that supported visible light activation, only WO_3 and Pt-C_3N_4 had energy band potentials (valence band at 3.2 V and 1.4 V respectively and conduction band at 0.2 V and -1.3 V respectively) that would facilitate OH radical formation either directly or indirectly as mentioned in reactions 2–6. Catalysts LaCr-$SrTiO_3$, Cr-$SrTiO_3$ and yellow TiO_2 (valence bands at 2.7 V, 2.7 V and 2.6 V respectively and conduction bands at -0.1 V for all the three photocatalysts) were selected to monitor if 7-hydroxycoumarin was formed even when the electronic structure of the catalyst was not suited to the redox potential of the reaction.

The photocatalytic hydroxylation of coumarin to 7-hydroxycoumarin over WO_3 and Pt-C_3N_4 under visible light is shown in Figure 4. As can be seen, minimal conversion of coumarin was observed over both Pt-C_3N_4 and WO_3, which was also supported by the low formation of 7-hydroxycoumarin (Figure 5). Pt-C_3N_4 displayed a slow yet steady conversion rate, reaching a 0.91 % drop in coumarin after 120 mins of irradiation whereas, a varying coumarin concentration pattern was seen over time on WO_3. It is interesting to note that there was an initial decrease in coumarin concentration followed by an increase which may be attributed to coumarin desorption from the surface of

WO_3. This desorption could be a result of the alteration in equilibrium in the closed system due to the possible evolution of O_2 from water on WO_3 under visible light.

Figure 4.

While the decrease in coumarin concentration is low, production of OH radicals over Pt-C_3N_4 and WO_3 was supported by the detection of 7-hydroxycoumarin upon photocatalysis (Figure 5). When WO_3 was used as the photocatalyst, there was no 7-hydroxycoumarin production until 30 minutes of irradiation which could be due to the rapid recombination of the electrons and the photo generated holes. After 30 minutes, OH radical production was steady with a gradual generation of 7-hydroxycoumarin being observed. In the case of Pt-C_3N_4 however, 7-hydroxycoumarin production was seen from 15 minutes. The initial increase in the 7-hydroxycoumarin concentration correlates to a rapid degradation of coumarin during the first 60 mins of irradiation.

Figure 5.

In contrast to Pt-C_3N_4 and WO_3, the catalysts LaCr-$SrTiO_3$, Cr-$SrTiO_3$ and yellow TiO_2 displayed no activity towards coumarin conversion to 7-hydroxycoumarin, which indicates no OH radical formation. Furthermore, under prolonged visible light irradiation no detectable 7-hydroxycoumarin was recorded.

3.2.3 Influence of photocatalysts' electronic structure and particle size on OH radical formation

In order to evaluate and discuss the performance of the catalysts, it is essential to consider the primary contributing factors; electronic structure and particle size. The electronic structure of the catalysts dictates the initial photo-excitation of electrons to higher energy levels, while the particle size dictates the concentration of photons absorbed and surface reactions between coumarin and OH radicals. As shown in reactions (2) – (6), OH radicals can occur via two routes in photocatalysis. The direct formation at the valence band requires a redox potential of 2.8 V vs NHE, while the indirect method occurs via the intermediate radical, $O_2^{\cdot -}$ and requires a redox potential of -0.33 V vs NHE [53]. The electronic structure of the catalysts tested in this study, in relation to the redox potentials required for radical formation, are shown in Figure 6.

Figure 6

As Figure 6 shows, catalysts TiO_2 P25, Pt-C_3N_4 and WO_3 possess an electronic structure which corresponds to the redox potential of OH radical formation via either direct or indirect mechanisms. The favourable electronic structure of TiO_2 for OH radical formation has been well documented and is evident from the results highlighted here. The performance of Pt-C_3N_4 and WO_3 for OH radical formation, however, has not been as well reported. The structure of WO_3 with a more positive valence band suggests it is capable of generating surface OH radicals, however, the results obtained indicate minimal 7-hydroxycoumarin production within 2 hours. Based on the structure, it was likely an increased rate of recombination preventing OH radical formation via the valence band hole, due to insufficient energy to initiate a reduction reaction at the conduction band [21]. To prevent recombination and to increase the OH radical production, Kim *et al*. synthesised Pt-doped WO_3 and found that the OH radical production from Pt-WO_3 was significantly higher than un-doped WO_3 [20]. Furthermore, the large particle size of approximately 100 nm for WO_3 indicates a smaller surface area, which leads to minimum absorption of light.

The electronic structure of Pt-C_3N_4 as seen from Figure 6 clearly indicates a reducing catalyst, which is also supported by its application in water reduction investigations [54]. Therefore, the hydroxylation of coumarin and subsequent formation of 7-hydroxycoumarin, as indicated by the earlier results, is likely via the indirect $O_2^{\cdot-}$ pathway. Based upon this observation, it is likely the low yield of OH radicals is a result of competition for the conduction band electron between superoxide formation and H^+ reduction to form H_2 (0 V vs NHE). In addition, since all these experiments were performed in a closed system with limited O_2, a reducing catalyst such as Pt-C_3N_4 is expected to produce less OH radicals than an open system. Furthermore, despite a favourable particle size of 20-40 nm, Pt-C_3N_4 was observed to agglomerate to form larger aggregates leading to a decrease in surface area and in turn light absorption.

In the case of LaCr-$SrTiO_3$, Cr-$SrTiO_3$ and yellow TiO_2, the electronic structures showed both the valence band and conduction band of all these catalysts to be lower than the redox potentials to facilitate radical formation as seen in Figure 6. These catalysts were primarily used as a control parameter to ensure no 7-hydroxycoumarin formation was observed.

The calculated OH radical concentrations and production rates produced over all catalysts screened are summarised in Table 1. The results show that the activity of the visible light activated photocatalysts studied were significantly lower than commercial P25 under UV light. This further emphasises that although there are numerous visible light absorbing photocatalysts, their ability to produce OH radicals is significantly lower than P25. In future, if any visible light absorbing photocatalysts are to be fabricated for the purpose of photocatalytic oxidation, their OH radical producing rates (and quantities) should be determined and compared to P25 as demonstrated here.

Table 1

4. CONCLUSION

The aim of screening UV and visible light absorbing photocatalysts to assess their oxidative strength was accomplished successfully by trapping OH radicals produced by the photocatalysts in 7-hydroxycoumarin. The OH radical production capabilities of various photocatalysts covering a range of band gaps and particle sizes were assessed by comparing and discussing their differences with the commercial UV light activated P25. To conclude, visible light activated photocatalysts such as LaCr-$SrTiO_3$, Cr-$SrTiO_3$ and yellow TiO_2 did not produce any OH radicals and this could be attributed to their electronic structure. Whereas, the (pseudo) maximum OH radical production rates of other visible light activated photocatalysts namely, WO_3 (0.28 µM/hr) and Pt-C_3N_4 (0.886 µM/hr) were found to be significantly lower when compared to the commercial UV light activated P25 photocatalyst (35.654 µM/hr). This method could be further exploited as novel photocatalysts are developed and to compare a range of P25 concentrations for OH radical production. This study further emphasises the challenges faced by the visible light photocatalysts for photocatalytic oxidation.

5. ACKNOWLEDGEMENTS

This work was supported by the Engineering and Physical Sciences Research Council (Project number EP/K036769/1), Robert Gordon University's IDEAS PhD studentship and Queen's University Belfast's PhD studentship. The author would also like to thank Professor A Prasanna de Silva, School of Chemistry and Chemical Engineering, Queen's University Belfast, for his valuable contribution during the progress meetings. Supporting data are openly available on Queen's University, Belfast Research Portal, http:// pure.qub.ac.uk/portal/en/datasets/search.html.

REFERENCES

[1] A. Fujishima, K. Honda, Electrochemical Photolysis of Water at a Semiconductor Electrode, Nature. 238 (1972) 37-38.

[2] D.W. Bahnemann, L.A. Lawton, P.K.J. Robertson, The Application of Semiconductor Photocatalysis for the Removal of Cyanotoxins from Water and Design Concepts for Solar Photocatalytic Reactors for Large Scale Water Treatment, in: S.L. Suib (Ed.), New and Future Developments in Catalysis, 1st ed., Elsevier, Amsterdam, 2013, pp. 395-415.

[3] M.R. Hoffmann, S.T. Martin, W. Choi, D.W. Bahnemann, Environmental Applications of Semiconductor Photocatalysis, Chem. Rev. 95 (1995) 69-96.

[4] P.K.J. Robertson, J.M.C. Robertson, D.W. Bahnemann, Removal of microorganisms and their chemical metabolites from water using semiconductor photocatalysis, J. Hazard. Mater. 211–212 (2012) 161-171.

[5] H. Kominami, S. Murakami, M. Kohno, Y. Kera, K. Okada, B. Ohtani, Stoichiometric decomposition of water by titanium(IV) oxide photocatalyst synthesized in organic media: Effect of synthesis and irradiation conditions on photocatalytic activity, Phys. Chem. Chem. Phys. 3 (2001) 4102-4106.

[6] C. McCullagh, P.K.J. Robertson, M. Adams, P.M. Pollard, A. Mohammed, Development of a slurry continuous flow reactor for photocatalytic treatment of industrial waste water, J. Photochem. Photobiol. A. 211 (2010) 42-46.

[7] P.K.J. Robertson, Semiconductor photocatalysis: an environmentally acceptable alternative production technique and effluent treatment process, J. Clean. Prod. 4 (1996) 203-212.

[8] M. Adams, I. Campbell, C. McCullagh, D. Russell, D.W. Bahnemann, P.K.J. Robertson, From Ideal Reactor Concepts to Reality: The Novel Drum Reactor for Photocatalytic Wastewater Treatment, Int. J. Chem. React. Eng. 11 (2013) 621-632.

[9] O. Carp, C.L. Huisman, A. Reller, Photoinduced reactivity of titanium dioxide, Progress in Solid State Chemistry. 32 (2004) 33-177.

[10] C. McCullagh, N. Skillen, M. Adams, P.K.J. Robertson, Photocatalytic reactors for environmental remediation: a review, J. Chem. Technol. Biotechnol. 86 (2011) 1002-1017.

[11] J. Jiang, Z. Zhou, V.K. Sharma, Occurrence, transportation, monitoring and treatment of emerging micro-pollutants in waste water — A review from global views, Microchem. J. 110 (2013) 292-300.

[12] A. Asghar, A.A. Abdul Raman, W.M.A. Wan Daud, Advanced oxidation processes for in-situ production of hydrogen peroxide/hydroxyl radical for textile wastewater treatment: a review, J. Clean. Prod. 87 (2015) 826-838.

[13] H. Fan, G. Li, F. Yang, L. Yang, S. Zhang, Photodegradation of cellulose under UV light catalysed by TiO2, J. Chem. Technol. Biotechnol. 86 (2011) 1107-1112.

[14] E. Szabó-Bárdos, K. Somogyi, N. Törő, G. Kiss, A. Horváth, Photocatalytic decomposition of l-phenylalanine over TiO2: Identification of intermediates and the mechanism of photodegradation, Appl. Catal. B: Environ. 101 (2011) 471-478.

[15] T. Hirakawa, K. Yawata, Y. Nosaka, Photocatalytic reactivity for O2− and OH radical formation in anatase and rutile TiO2 suspension as the effect of H2O2 addition, Appl. Catal. A-Gen. 325 (2007) 105-111.

[16] Y. Nosaka, T. Daimon, A.Y. Nosaka, Y. Murakami, Singlet oxygen formation in photocatalytic TiO2 aqueous suspension, Phys. Chem. Chem. Phys. 6 (2004) 2917-2918.

[17] X. Yan, T. Ohno, K. Nishijima, R. Abe, B. Ohtani, Is methylene blue an appropriate substrate for a photocatalytic activity test? A study with visible-light responsive titania, Chemical Physics Letters. 429 (2006) 606-610.

[18] B. Ohtani, Preparing Articles on Photocatalysis—Beyond the Illusions, Misconceptions, and Speculation, Chem. Lett. 37 (2008) 216-229.

[19] A. Mills, An overview of the methylene blue ISO test for assessing the activities of photocatalytic films, Applied Catalysis B: Environmental. 128 (2012) 144-149.

[20] J. Kim, C.W. Lee, W. Choi, Platinized WO3 as an Environmental Photocatalyst that Generates OH Radicals under Visible Light, Environ. Sci. Technol. 44 (2010) 6849-6854.

[21] Q. Xiang, J. Yu, P.K. Wong, Quantitative characterization of hydroxyl radicals produced by various photocatalysts, J. Colloid Interface Sci. 357 (2011) 163-167.

[22] M. Sato, T. Ohgiyama, J.S. Clements, Formation of chemical species and their effects on microorganisms using a pulsed high voltage discharge in water, Industry Applications Society Annual Meeting. 2 (1994) 1455-1461.

[23] H. Czili, A. Horváth, Applicability of coumarin for detecting and measuring hydroxyl radicals generated by photoexcitation of TiO2 nanoparticles, Appl. Catal. B: Environ. 81 (2008) 295-302.

[24] R. Ono, T. Oda, Measurement of hydroxyl radicals in pulsed corona discharge, J. Electrostatics. 55 (2002) 333-342.

[25] W. Hoeben, E. van Veldhuizen, W. Rutgers, G. Kroesen, Gas phase corona discharges for oxidation of phenol in an aqueous solution, J. Phys. D: Appl. Phys. 32 (1999) 133-137.

[26] P. Sunka, V. Babický, M. Clupek, P. Lukes, M. Simek, J. Schmidt, M. Cern, Generation of chemically active species by electrical discharges in water, Plasma Sources Sci. Technol. 8 (1999) 258-265.

[27] B. Sun, M. Sato, J. Sid Clements, Optical study of active species produced by a pulsed streamer corona discharge in water, J. Electrostatics. 39 (1997) 189-202.

[28] M.G. Steiner, C.F. Babbs, Quantitation of the hydroxyl radical by reaction with dimethyl sulfoxide, Arch. Biochem. Biophys. 278 (1990) 478-481.

[29] M. Sahni, B.R. Locke, Quantification of Hydroxyl Radicals Produced in Aqueous Phase Pulsed Electrical Discharge Reactors, Ind. Eng. Chem. Res. 45 (2006) 5819-5825.

[30] J. Ku, E. Zimowski, United States Department of Labor, Occupational Safety and Health Administration. 3M Formaldehyde Monitor (Model 3721), Product evaluation (PE-10). 205 (1989).

[31] S.A.V. Eremia, D. Chevalier-Lucia, G. Radu, J. Marty, Optimization of hydroxyl radical formation using TiO2 as photocatalyst by response surface methodology, Talanta. 77 (2008) 858-862.

[32] T. Maezono, M. Tokumura, M. Sekine, Y. Kawase, Hydroxyl radical concentration profile in photo-Fenton oxidation process: Generation and consumption of hydroxyl radicals during the discoloration of azo-dye Orange II, Chemosphere. 82 (2011) 1422-1430.

[33] M. Tokumura, R. Morito, R. Hatayama, Y. Kawase, Iron redox cycling in hydroxyl radical generation during the photo-Fenton oxidative degradation: Dynamic change of hydroxyl radical concentration, Appl. Catal. B: Environ. 106 (2011) 565-576.

[34] S. Kanazawa, T. Furuki, T. Nakaji, S. Akamine, R. Ichiki, Measurement of OH Radicals in Aqueous Solution Produced by Atmospheric-pressure LF Plasma Jet, I. J. PEST. 6 (2012) 166-171.

[35] K. Ishibashi, A. Fujishima, T. Watanabe, K. Hashimoto, Quantum yields of active oxidative species formed on TiO2 photocatalyst, J. Photochem. Photobiol. A. 134 (2000) 139-142.

[36] T. Hirakawa, Y. Nosaka, Properties of O2.- and OH. Formed in TiO2 Aqueous Suspensions by Photocatalytic Reaction and the Influence of H2O2 and Some Ions, Langmuir. 18 (2002) 3247-3254.

[37] Z. Li, T. Liang, S. Lv, Q. Zhuang, Z. Liu, A Rationally Designed Upconversion Nanoprobe for in Vivo Detection of Hydroxyl Radical, J. Am. Chem. Soc. 137 (2015) 11179-11185.

[38] J. Zhang, Y. Nosaka, Quantitative Detection of OH Radicals for Investigating the Reaction Mechanism of Various Visible-Light TiO2 Photocatalysts in Aqueous Suspension, J. Phys. Chem. C. 117 (2013) 1383-1391.

[39] M.E. Lindsey, M.A. Tarr, Quantitation of hydroxyl radical during Fenton oxidation following a single addition of iron and peroxide, Chemosphere. 41 (2000) 409-417.

[40] J. Zhang, Y. Nosaka, Generation of OH radicals and oxidation mechanism in photocatalysis of WO3 and BiVO4 powders, J. Photochem. Photobiol. A. 303–304 (2015) 53-58.

[41] F. Fina, H. Menard, J.T.S. Irvine, The effect of Pt NPs crystallinity and distribution on the photocatalytic activity of Pt-g-C3N4, Phys. Chem. Chem. Phys. 17 (2015) 13929-13936.

[42] C. Randorn, J.T.S. Irvine, P. Robertson, Synthesis of Visible-Light-Activated Yellow Amorphous Photocatalyst, Int. J. Photoenergy. 2008 (2008) 1-6.

[43] S. Ouyang, H. Tong, N. Umezawa, J. Cao, P. Li, Y. Bi, Y. Zhang, J. Ye, Surface-Alkalinization-Induced Enhancement of Photocatalytic H2 Evolution over SrTiO3-Based Photocatalysts, J. Am. Chem. Soc. 134 (2012) 1974-1977.

[44] M. Muralidharan, V. Anbarasu, A. Elaya Perumal, K. Sivakumar, Carrier mediated ferromagnetism in Cr doped SrTiO3 compounds, J. Mater. Sci. : Mater. Electron. 26 (2015) 6352-6365.

[45] J. Guo, Y. Li, S. Zhu, Z. Chen, Q. Liu, D. Zhang, W. Moon, D. Song, Synthesis of WO3@Graphene composite for enhanced photocatalytic oxygen evolution from water, RSC Adv. 2 (2012) 1356-1363.

[46] K. van Benthem, C. Elsässer, R.H. French, Bulk electronic structure of SrTiO3: Experiment and theory, J. Appl. Phys. 90 (2001) 6156-6164.

[47] J. Kamalakkannan, V.L. Chandraboss, S. Prabha, S. Senthilvelan, Advanced construction of heterostructured InCrO4-TiO2 and its dual properties of greater UV-photocatalytic and antibacterial activity, RSC Adv. 5 (2015) 77000-77013.

[48] M. Wojtoniszak, B. Zielinska, R.J. Kalenczuk, E. Mijowska, Photocatalytic performance of titania nanospheres deposited on graphene in coumarin oxidation reaction, Materials Science-Poland. 30 (2012) 32-38.

[49] G. Li, K.H. Wong, X. Zhang, C. Hu, J.C. Yu, R.C.Y. Chan, P.K. Wong, Degradation of Acid Orange 7 using magnetic AgBr under visible light: The roles of oxidizing species, Chemosphere. 76 (2009) 1185-1191.

[50] J. Zhang, Y. Nosaka, Mechanism of the OH Radical Generation in Photocatalysis with TiO2 of Different Crystalline Types, J. Phys. Chem. C. 118 (2014) 10824-10832.

[51] H. Guan, L. Zhu, H. Zhou, H. Tang, Rapid probing of photocatalytic activity on titania-based self-cleaning materials using 7-hydroxycoumarin fluorescent probe, Anal. Chim. Acta. 608 (2008) 73-78.

[52] Z. Huang, Q. Sun, K. Lv, Z. Zhang, M. Li, B. Li, Effect of contact interface between TiO2 and g-C3N4 on the photoreactivity of g-C3N4/TiO2 photocatalyst: (0 0 1) vs (1 0 1) facets of TiO2, Applied Catalysis B: Environmental. 164 (2015) 420-427.

[53] P.M. Wood, The potential diagram for oxygen at pH 7, Biochem. J. 253 (1988) 287-289.

[54] G. Zhang, Z. Lan, L. Lin, S. Lin, X. Wang, Overall water splitting by Pt/g-C3N4 photocatalysts without using sacrificial agents, Chem. Sci. 7 (2016) 3062-3066.

List of Captions for figures and tables.

Figure 1: XRD profiles of photocatalysts representing the plane indices [44,45].

Figure 2: UV-Visible absorption spectra of photocatalysts

Figure 3: Coumarin and 7-hydroxycoumarin profiles of 100 ml of 100 µM coumarin with 0.1 g/L P25 under 36 W UV light

Figure 4: Coumarin profiles of 100 ml of 100 µM coumarin with 0.1 g/L visible light photocatalysts; Inset: coumarin profiles of WO_3 and Pt-C_3N_4

Figure 5: 7-hydroxycoumarin production profiles of 100 ml of 100 µM coumarin with 0.1 g/L visible light photocatalysts

Figure 6: Electronic structure of the photocatalysts used

Table 1: Pseudo maximum OH radical production rates and quantities.

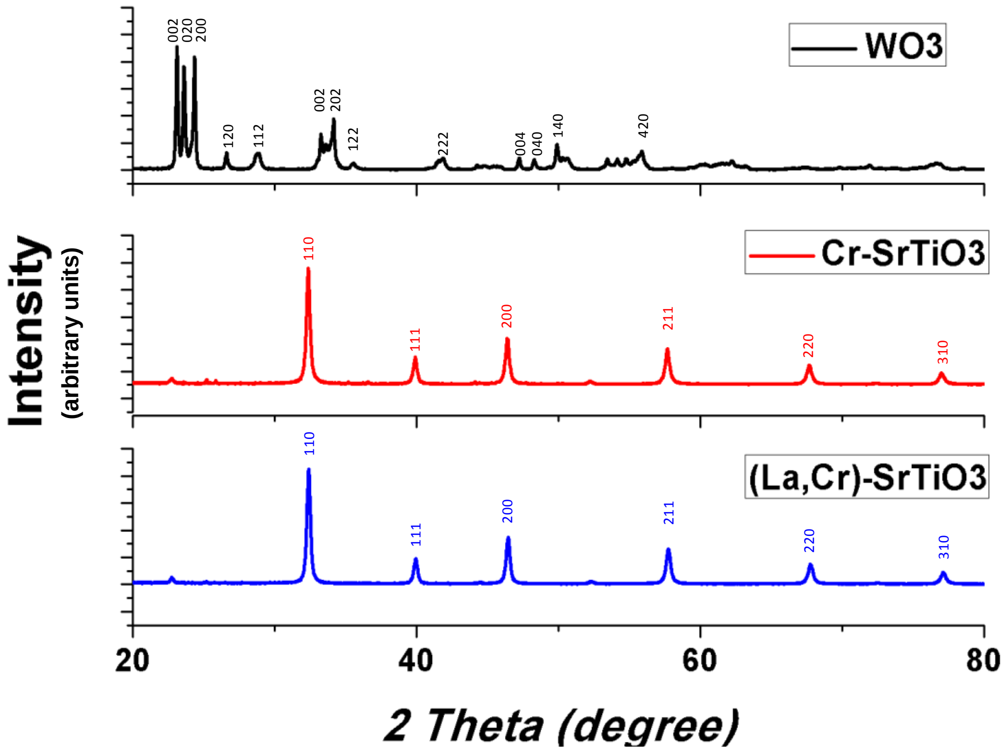

WO3
002
020
200
120
112
002
202
122
222
004
040
140
420
Cr-SrTiO3
110
111
200
211
220
310
(La,Cr)-SrTiO3
110
111
200
211
220
310
Intensity
(arbitrary units)
20
40
60
80
2 Theta (degree)

Figure 1

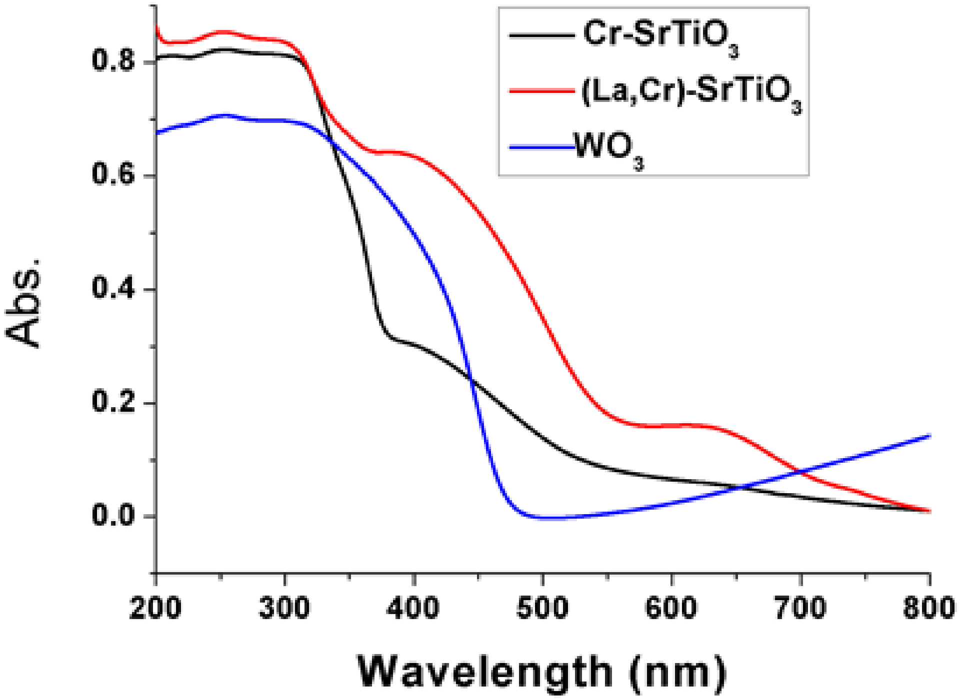
Cr-SrTiO$_3$
(La,Cr)-SrTiO$_3$
WO$_3$
Abs.
0.0
0.2
0.4
0.6
0.8
200
300
400
500
600
700
800
Wavelength (nm)

Figure 2

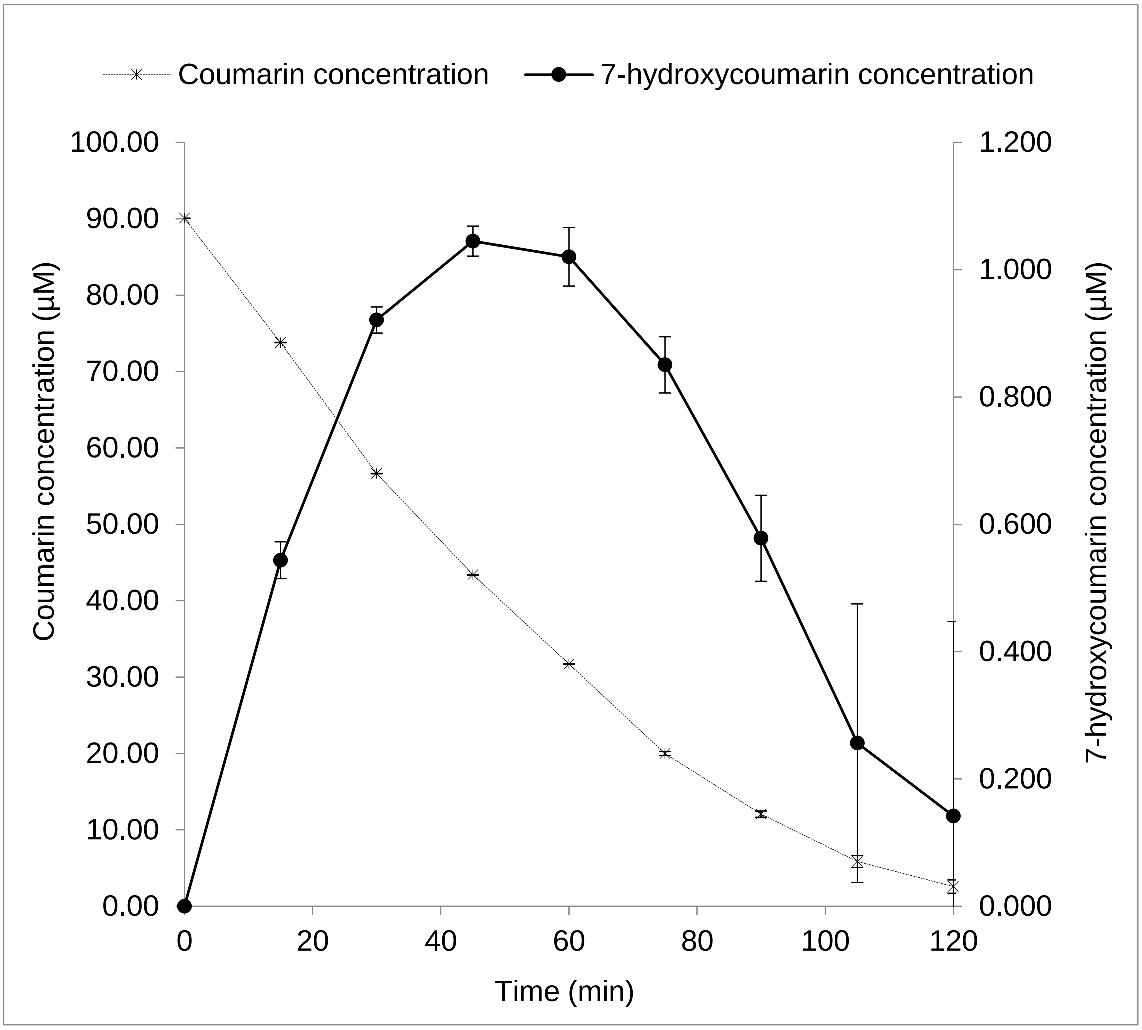
Coumarin concentration
7-hydroxycoumarin concentration
Coumarin concentration (µM)
7-hydroxycoumarin concentration (µM)
Time (min)
100.00
90.00
80.00
70.00
60.00
50.00
40.00
30.00
20.00
10.00
0.00
1.200
1.000
0.800
0.600
0.400
0.200
0.000
0
20
40
60
80
100
120

Figure 3

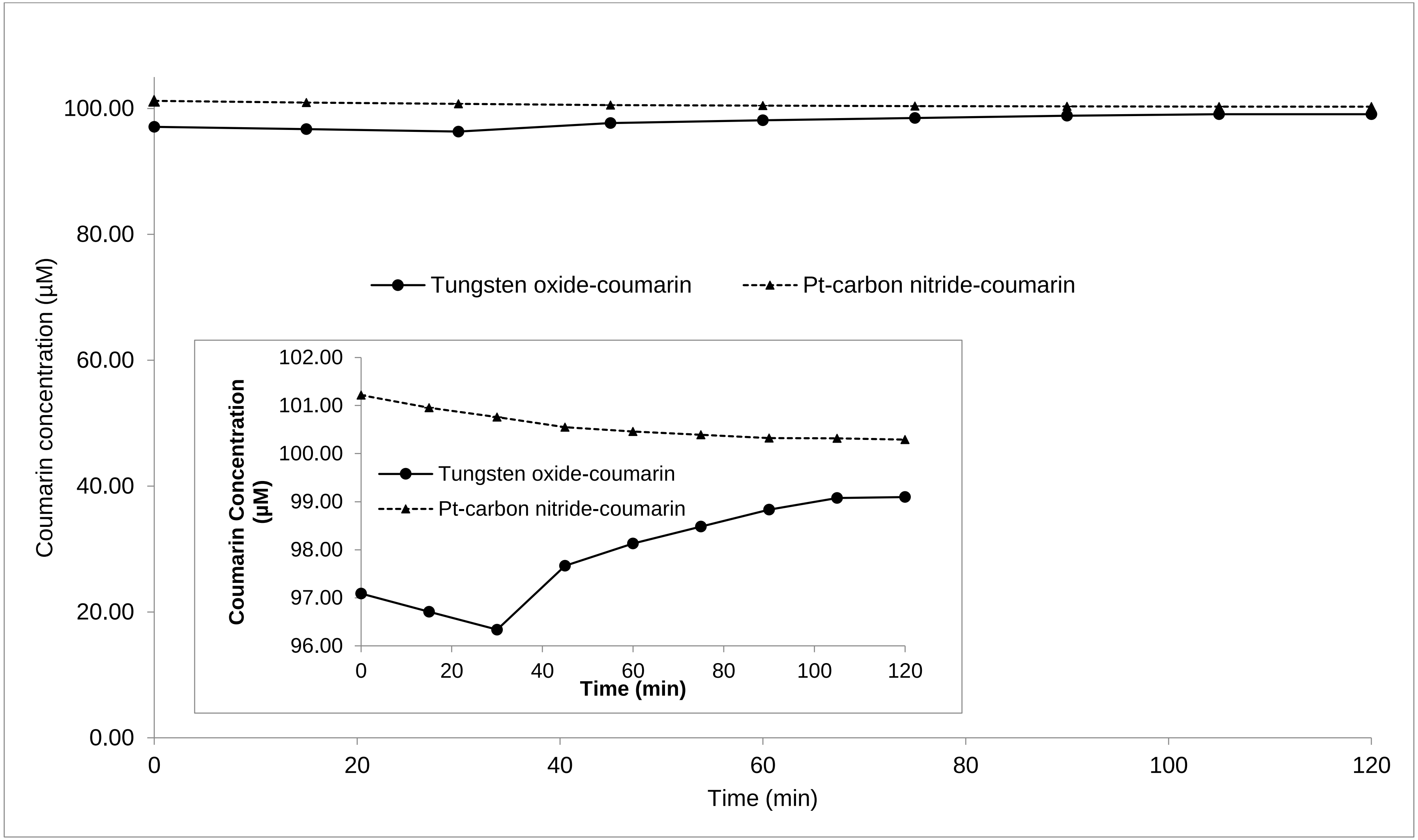
Coumarin concentration (µM)
100.00
80.00
60.00
40.00
20.00
0.00
0
20
40
60
80
100
120
Time (min)
Tungsten oxide-coumarin
Pt-carbon nitride-coumarin
Coumarin Concentration (µM)
102.00
101.00
100.00
99.00
98.00
97.00
96.00
0
20
40
60
80
100
120
Time (min)
Tungsten oxide-coumarin
Pt-carbon nitride-coumarin

Figure 4

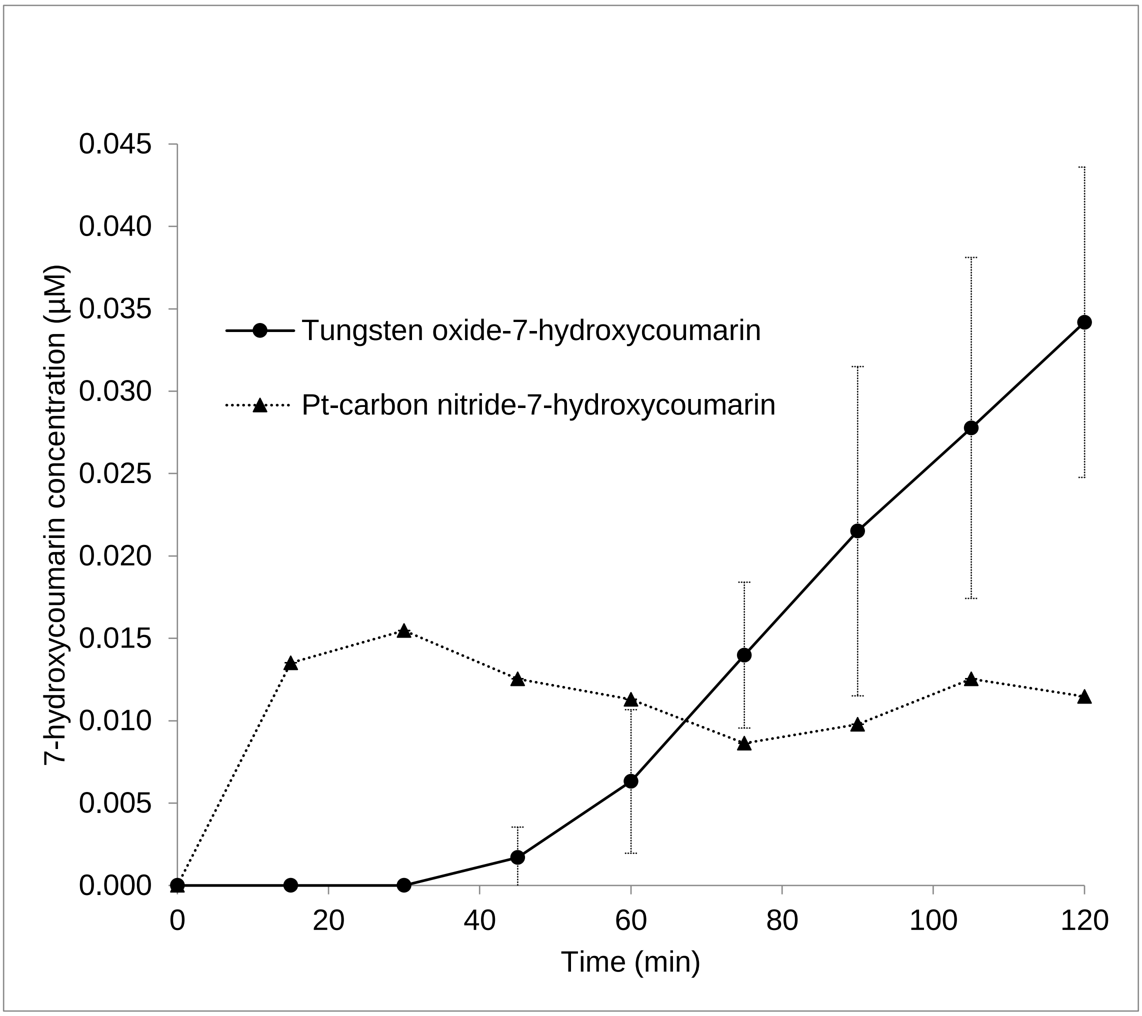
0.045
0.040
0.035
0.030
0.025
0.020
0.015
0.010
0.005
0.000
7-hydroxycoumarin concentration (µM)
0
20
40
60
80
100
120
Time (min)
Tungsten oxide-7-hydroxycoumarin
Pt-carbon nitride-7-hydroxycoumarin

Figure 5

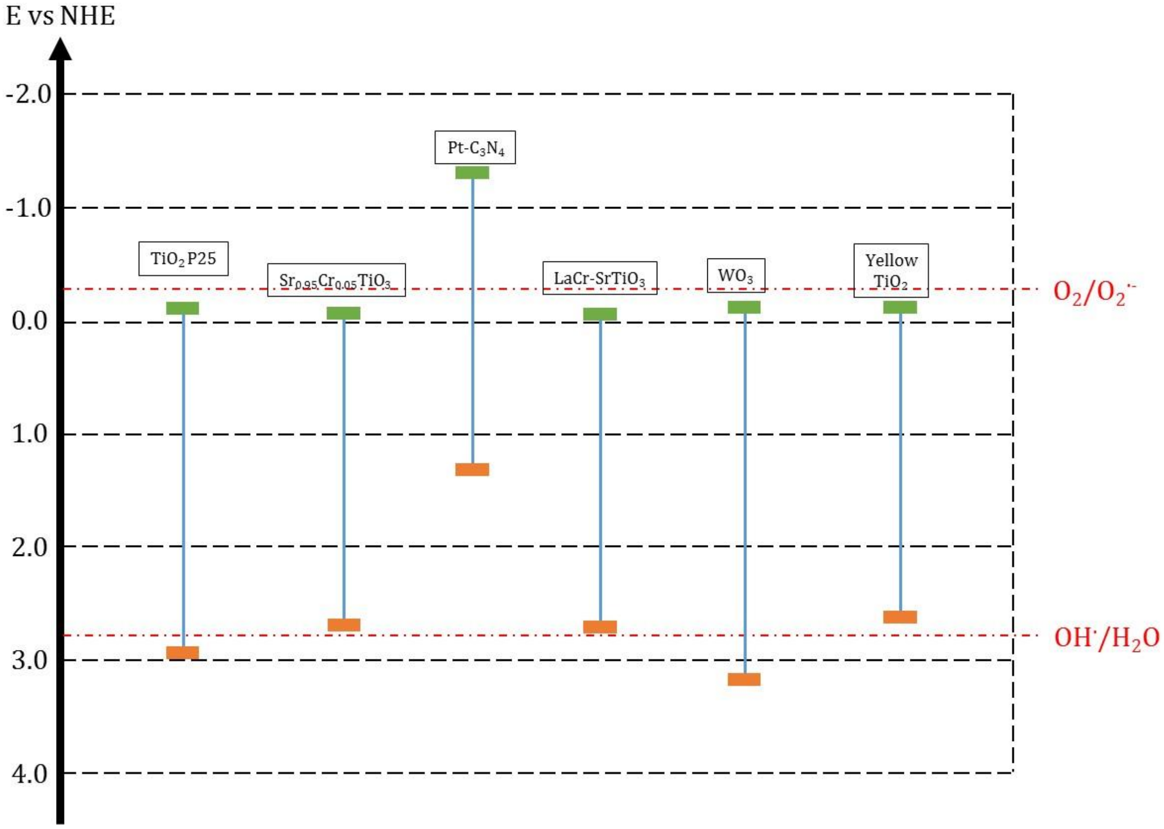
E vs NHE
-2.0
-1.0
0.0
1.0
2.0
3.0
4.0
TiO_2 P25
$Sr_{0.95}Cr_{0.05}TiO_3$
Pt-C_3N_4
LaCr-$SrTiO_3$
WO_3
Yellow TiO_2
$O_2/O_2^{\cdot -}$
$OH^{\cdot}/H_2O$

Figure 6

Photocatalyst	Light Source	Maximum OH radical concentration (μM)	Time at which maximum concentration of OH radical was produced (min)	Maximum OH radical production rate (μM/hr)
P25	UV	16.9	45	35.654
WO_3	visible	0.560	120	0.280
Pt-C_3N_4	visible	0.254	30	0.886

Table 1